Rare Met.
https://doi.org/10.1007/s12598-024-02871-x

RARE METALS

ORIGINAL ARTICLE

A novel Au(III) agent designed to inhibit tumor growth and metastasis through inducing immunogenic cell death

Wen-Juan Li, Shan-He Li, Xue-Yu Man, Gang Xu, Zhen-Lei Zhang, Yao Zhang, Hong Liang*, Feng Yang*

Received: 31 December 2023 / Revised: 4 March 2024 / Accepted: 18 March 2024
© Youke Publishing Co., Ltd. 2024

Abstract To treat cancer and inhibit its metastasis to the greatest extent, we proposed to develop an Au(III) agent to induce immunogenic cell death (ICD) and establish long-term immunity. To this end, we optimized a series of Au(III) 2-benzoylpyridine thiosemicarbazone complexes to obtain an Au(III) agent (5b) with excellent cytotoxicity to cancer. The results show that 5b effectively inhibits tumor growth and its metastasis in vivo. Interestingly, we revealed a new mechanism of 5b inhibiting tumor growth and metastasis: 5b releases ICD-related damage-associated molecular patterns (DAMPs), such as calreticulin (CRT), ATP and high mobility group box 1 (HMGB1) by inducing endoplasmic reticulum stress (ERS) and mitochondrial dysfunction, which then stimulated an antitumor $CD8^+$ T cell response and $Foxp3^+$ T cell depletion, thus establishing long-action antitumor immunity.

Supplementary Information The online version contains supplementary material available at https://doi.org/10.1007/s12598-024-02871-x.

W.-J. Li, S.-H. Li, X.-Y. Man, G. Xu, Z.-L. Zhang, Y. Zhang, H. Liang*, F. Yang*
State Key Laboratory for Chemistry and Molecular Engineering of Medicinal Resources, Key Laboratory for Chemistry and Molecular Engineering of Medicinal Resources (Ministry of Education of China), Collaborative Innovation Center for Guangxi Ethnic Medicine, School of Chemistry and Pharmaceutical Sciences, Guangxi Normal University, Guilin 541004, China
e-mail: hliang@mailbox.gxnu.edu.cn

F. Yang
e-mail: fyang@mailbox.gxnu.edu.cn

Y. Zhang
Department of Biochemistry and Molecular Biology, Michigan State University, East Lansing 48824, USA

Keywords Gold complex; Anticancer; Thiosemicarbazone; Endoplasmic reticulum stress; Immunogenic cell death

1 Introduction

Cancer has emerged as one of the deadliest diseases worldwide in recent decades, and it is a complex disease that is difficult to cure and is prone to metastasis [1]. *Cisplatin* is the first platinum (Pt)-based anticancer drug approved by the Food and Drug Administration (FDA) for cancer treatment. Still, long-term survival in patients remains disappointing because cisplatin not only kills cancer cells through a single mechanism of action on DNA but also cannot inhibit cancer recurrence or metastasis [2]. Therefore, to more effectively treat cancer, on the one hand, we can develop novel non-Pt anticancer drugs with different mechanisms of action and pharmaceutical profiles to overcome the shortcomings of *cisplatin*; on the other hand, we can combine multiple treatment modalities for cancer treatment, such as integration of chemotherapy and immunotherapy.

Immunotherapy provides a considerable opportunity to treat malignant tumors, and it has attracted significant attention for cancer treatment currently [3]. Immunogenic cell death (ICD) is a specific type of regulated cell death sufficient for activating an adaptive immune response against dead or dying cell antigens, thus eliciting the long-term efficacy of anticancer drugs by directly killing cancer cells and activating antitumor immunity [4, 5]. The ICD-inducing capacity is closely related to endoplasmic reticulum stress (ERS) induction and reactive oxygen species (ROS) generation [6]. Anticancer agents that induce ICD are promising for improving treatment using immune

Published online: 22 July 2024

checkpoint inhibitors and may become the mainstay of cancer treatment in the future [7, 8]. Currently, several metal anticancer agents, such as gold complexes, Pt complexes, copper complexes and iridium complexes, have been demonstrated to serve as potential ICD inducers. Liu's group demonstrated a variety of NHC-Au(I) complexes can effectively induce ICD for cancer therapy [9, 10]. Arambula et al. also rationally designed an Au(I) bis-NHC complex as an ICD inducer and highlighted a novel strategy that can be used to prepare asymmetric redox-active Au(I) bis-NHC complexes [11]. Zou et al. classified the mechanisms underlying the drug-induced ICD in detail [12]. They also reported an ERS-inducing cyclometalated Ir(III) − bisNHC complex as a ICD inducer, which is the first biotarget study of a metal-based agent that mechanistically bridges GRP78 and ICD [13]. Kaur et al. [14] proved a copper-(II) complex containing a polypyridyl ligand and a Schiff base ligand could trigger ICD in breast cancer stem cells. However, only a few chemotherapeutics, oncolytic viruses and other treatment modalities can trigger ICD and provide long-term clinical benefits [15, 16]. Thus, exploiting more potential ICD inducers would address a critical need.

On the one hand, quantities of Au(III) complexes have exhibited excellent anticancer activities not only by the generation of ROS to trigger apoptosis of cancer cells, but also by the accumulation of unfolded proteins to induce ERS, which are potential markers of ICD-induced effects; on the other hand, metal thiosemicarbazone complexes have attracted increasing attention as potential anticancer agents because they inhibit tumor growth by combining chemotherapy with immunotherapy [17, 18]. Thus, we propose to design a new Au(III) thiosemicarbazone complex that induces an ICD effect to inhibit tumor growth and metastasis effectively.

Based on these considerations, to effectively cure cancer and inhibit tumor metastasis, we propose to design an Au(III) thiosemicarbazone complex to activate immune response by inducing ICD. For this purpose, we designed and synthesized a series of Au(III) 2-benzoylpyridine thiosemicarbazone complexes (1b–5b) and obtained an Au(III) complex (5b) with excellent cytotoxicity to cancer cells. Subsequently, we not only studied the anti-tumor and anti-metastasis behavior of 5b in vitro and in vivo but also confirmed the anticancer mechanisms of 5b.

2 Experimental

2.1 Materials

All chemicals and solvents were purchased from Innochem Company (Shanghai, China) or Sigma-Aldrich. All ligands (1a–5a) were obtained by the previously reported method of our group [19]. All the target complexes used in these experiments were of high purity (≥ 95%) and stable under physiological pH conditions, as determined by ultraviolet–visible (UV–Vis) spectra (Fig. S1). All cell lines were purchased from the Shanghai Institute for Biological Science, Chinese Academy of Sciences. All the antibodies used in western blotting were supplied by Abcam (Cambridge, UK). UV–Vis spectra were obtained using a UV–Vis spectrophotometer by Shimadzu (UV-2600).

2.2 Synthesis of Au(III) complexes (1b–5b)

The Au(III) complexes (1b–5b) were synthesized by reaction of ligands (1a–5a) with $Na[AuCl_4]\cdot 2H_2O$. In brief, the ligands (0.3 mmol) and $Na[AuCl_4]\cdot 2H_2O$ (0.3 mmol) were dissolved in methanol (15 ml) and stirred at 30 °C for 2 h. After filtration and vacuum drying, a brown solid was obtained and dissolved in dichloromethane (5 ml). Subsequently, the solution was dripped into a 20 ml test tube, and then n-hexane (10 ml) was added slowly. The crystals of Au(III) complexes (deep red crystal) were acquired by diffusion and evaporated at room temperature for a week. The structures were characterized by electrospray ionization-mass spectrometry (ESI–MS) (Figs. S9–S13), X-ray crystallography, infrared spectrum analysis (Figs. S14–S18) and 1hydrogen-nuclear magnetic resonance (^{1}H-NMR) (Figs. S24–S28).

2.2.1 Complex 1b

Yield: 42%, Anal. Calcd (%) for $C_{13}H_{11}Cl_5N_4Au_2S$: C, 18.89; H, 1.34; N, 6.78; S, 3.88. IR (KBr): 3359 (s, amide), 3276 (s, NH), 3181 (m, aromatic hydrogen), 1613 (s), 1535 (s), 1506 (s, aromatic), 1329 (m, C=N), 1156 (s, thioamide), 782 (m, C-H), 691 (m, C=S), 518 (m) cm^{-1}. ^{1}H NMR (400 MHz, DMSO-d_6) δ 9.42 (s, 1H), 9.15 (s, 1H), 9.03 (dd, J = 5.6, 1.2 Hz, 1H), 8.40 (td, J = 7.9, 1.5 Hz, 1H), 8.06–7.97 (m, 1H), 7.68 (dd, J = 5.2, 1.9 Hz, 3H), 7.61–7.52 (m, 2H), 7.47 (dd, J = 8.0, 1.0 Hz, 1H). ESI–MS: m/z = 487.00 [M-$AuCl_4$].

2.2.2 Complex 2b

Yield: 48%, Anal. Calcd (%) for $C_{14}H_{13}Cl_3N_4Au_2S$: C, 21.85; H, 1.70; N, 7.28; S, 4.17. IR (KBr): 3266 (s, amide), 3070 (s, NH), 3023 (m, aromatic hydrogen), 1581 (s), 1520 (s), 1458 (s, aromatic), 1305 (m, C=N), 1106 (s, thioamide), 778 (m, C-H), 691 (m, C=S), 643 (m) cm^{-1}. ^{1}H NMR (400 MHz, DMSO-d_6) δ 9.58 (d, J = 4.7 Hz, 1H), 9.04 (d, J = 5.4 Hz, 1H), 8.46–8.34 (m, 1H), 8.08–7.92 (m, 1H), 7.65 (ddd, J = 17.0, 7.5, 3.4 Hz, 6H), 2.88 (s, 3H). ESI–MS: m/z = 501.02 [M-$AuCl_2$].

2.2.3 Complex 3b

Yield: 55%, Anal. Calcd (%) for $C_{19}H_{15}Cl_3N_4Au_2S$: C, 27.44; H, 1.82; N, 6.74; S, 3.85. IR (KBr): 3279 (s, amide), 3193 (s, NH), 3082 (m, aromatic hydrogen), 1599 (s), 1549 (s), 1510 (s, aromatic), 1266 (m, C=N), 1127 (s, thioamide), 967 (m, C-H), 758 (m, C=S), 699 (m) cm^{-1}. ^1H NMR (400 MHz, DMSO-d6) δ 11.53 (s, 1H), 9.11 (d, J = 4.6 Hz, 1H), 8.47 (td, J = 7.9, 1.3 Hz, 1H), 8.10 (ddd, J = 7.5, 5.7, 1.2 Hz, 1H), 7.85–7.62 (m, 6H), 7.35–7.20 (m, 4H), 7.15 (d, J = 6.4 Hz, 1H). ESI–MS: m/z = 563.04 [M-$AuCl_2$].

2.2.4 Complex 4b

Yield: 48%, Anal. Calcd (%) for $C_{17}H_{17}Cl_3N_4Au_2S$: C, 25.22; H, 2.12; N, 6.92; S, 3.96. IR (KBr): 3279 (s, amide), 3193 (s, NH), 3082 (m, aromatic hydrogen), 1599 (s), 1549 (s), 1510 (s, aromatic), 1266 (m, C=N), 1127 (s, thioamide), 967 (m, C–H), 758 (m, C=S), 699 (m) cm^{-1}. ^1H NMR (400 MHz, DMSO-d_6) δ 9.04 (dd, J = 5.6, 1.2 Hz, 1H), 8.40 (td, J = 7.9, 1.5 Hz, 1H), 7.98 (ddd, J = 7.6, 5.6, 1.3 Hz, 1H), 7.69–7.58 (m, 6H), 3.52 (dt, J = 27.1, 6.6 Hz, 4H), 1.95 (dp, J = 19.9, 6.6 Hz, 4H). ESI–MS: m/z = 541.05 [M-$AuCl_2$].

2.2.5 Complex 5b

Yield: 50%, Anal. Calcd (%) for $C_{15}H_{15}Cl_3N_4Au_2S$: C, 22.99; H, 1.93; N, 7.15; S, 4.09. IR (KBr): 3319 (s, amide), 3268 (s, NH), 3059 (m, aromatic hydrogen), 1541 (s), 1501 (s), 1429 (s, aromatic), 1338 (m, C=N), 1133 (s, thioamide), 901 (m, C–H), 778 (m, C=S), 687 (m) cm^{-1}. ^1H NMR (400 MHz, DMSO-d_6) δ 9.04 (dd, J = 5.6, 1.2 Hz, 1H), 8.40 (td, J = 7.9, 1.4 Hz, 1H), 7.99 (ddd, J = 7.5, 5.6, 1.3 Hz, 1H), 7.70–7.64 (m, 3H), 7.61 (dd, J = 7.0, 3.0 Hz, 3H), 3.22 (s, 6H). ESI–MS: m/z = 515.04 [M-$AuCl_2$].

2.3 Cytotoxicity assay

SK-OV-3 cells were seeded in 96-well plates at a density of 5×10^3 cells/well and pre-cultured for 24 h. Subsequently, different concentrations of compounds were added, and they were incubated for another 48 h. Then, 10 μL 3-(4,5-dimethylthiazol-2-yl)-2,5-diphenyl-tetrazolium bromide (MTT) solution (5 $mg{\cdot}ml^{-1}$) was added to each well and incubated for 4 h. After removing the media, 100 μL DMSO solution was added and mixed thoroughly. Finally, the absorbance at the absorption wavelength of 570/630 nm was measured using an enzyme labeling instrument, and the IC_{50} values of each complex were calculated.

2.4 In vivo animal experiments

All animal experiments carried out in this study received approval from the Chinese Academy of Sciences Institutional Animal Care and Use Committee. Healthy female C57BL/6J mice (aged for 6–7 weeks old and weighting 18–22 g) were obtained from Hunan SJA Laboratory Animal Co., Ltd. (Hunan, China, Approval no. SCXK 2019–0004). The Institutional Animal Ethical Committee (IAEC) project number for this study is No. 20200405–001.

2.5 In vivo anti-tumor efficacy

After the tumor volumes reached $\sim$ 80 mm^3, mice with a uniform tumor size were randomly divided into three groups (n = 5). The mice were injected with 0.9% NaCl and 5b at 2 or 4 $\mu mol{\cdot}kg^{-1}$ every 2 days for 27 days. Body weight and tumor size were recorded every 2 days. At the end of the treatment, the mice were sacrificed, and the tumor tissues and main organs were obtained for hematoxylin and eosin (H&E), terminal deoxynucleotidyl transferase-mediated dUTP-biotin nick end labeling (TUNEL) staining, immunofluorescence and immunohistochemical analyses.

2.6 In vivo anti-metastasis experiments

Briefly, the lung metastatic model was established by intravenous injection of ovarian cancer cells (2×10^5 cells per mouse) via the tail vein. The mice were treated with 5b every 2 days. The mice were sacrificed at the end of treatment, and the lungs were collected for weighting and H&E staining.

2.7 Statistical analysis

Data of all measurements are presented as mean ± standard deviation (SD). Differences were considered to be statistically significant if the p value < 0.05.

3 Results

3.1 Design and structures of five Au(III) complexes

Thiosemicarbazone compounds have attracted considerable attention owing to their excellent chelating properties and biological activity [20]. On the one hand, modification of the N-4 position of thiosemicarbazone compounds can effectively increase the lipophilicity of the compounds, thereby improving their antitumor activity; on the other hand, rationally combining metal ions can achieve "1 + 1 > 2"

antitumor efficacy [21]. Thus, we designed and synthesized a series of 2-benzoylpyridine thiosemicarbazone compounds by modifying the hydrogen atom(s) with other group(s) at the N4-position (1a–5a) and the corresponding Au(III) complexes (1b–5b). The crystal structures of the Au(III) 2-benzoylpyridine thiosemicarbazone complexes were characterized by X-ray crystallography (Fig. 1). X-ray crystallography analysis revealed that the five Au(III) complexes are monoclinic crystal systems. The partial bond lengths and bond angles of the crystal structures of the complexes are shown in Tables S1, S2.

3.2 Cytotoxicity of Au(III) complexes in vitro

The MTT assay was used to detect the in vitro cytotoxicity of the 2-benzoylpyridine thiosemicarbazone compounds (1a–5a) and the corresponding Au(III) complexes (1b–5b) against various cell lines, such as human glioblastoma cells (T98G), human osteosarcoma cells (143B), human malignant melanoma (A375), human ovarian cancer (SK-OV-3) and human proximal tubular epithelial cells (HK-2). As listed in Table 1, the half-maximal inhibitory concentration (IC_{50}) of ligands (1a–5a) against cancer cells was higher than that of the Au(III) complexes (IC_{50} = 1.05 − 23.01 μM), indicating that the coordination of Au-iron had effectively improved the cytotoxicity of the complexes. Meanwhile, the cytotoxicities of 2b and 3b against SK-OV-3 cells were ∼ twofold higher than that of 1b when modified with a methyl (2b) or benzene ring (3b) at the N-4 position of 1b. The cytotoxicity of 4b showed a sixfold increase when the N-4 position of 1b formed a piperidine ring. The Au(III) complex modified with two methyl groups (5b) at the N-4 position of 1b showed the most potent cytotoxicity against SK-OV-3 cells (IC_{50} = (1.05 ± 0.68) μM), which was ∼ 17-fold higher than that of 1b (IC_{50} = (17.43 ± 1.02) μM).

3.3 In vitro antiproliferative activity of 5b

Colony formation assays were performed to investigate the effect of 5b on the proliferative ability of SK-OV-3 cells. It was shown that 5b could inhibit SK-OV-3 cell colony formation in a concentration-dependent manner (Fig. 2a). In addition, multicellular spheroids (MCSs) of SK-OV-3 cells were constructed to characterize the anticancer activity of 5b under more challenging and biologically relevant conditions. As shown in Fig. 2b, the MCSs in the control group remained intact, and the size of spheroids either did not change or slightly increased. In contrast, the MCSs treated with 5b became loose, and the cells on the

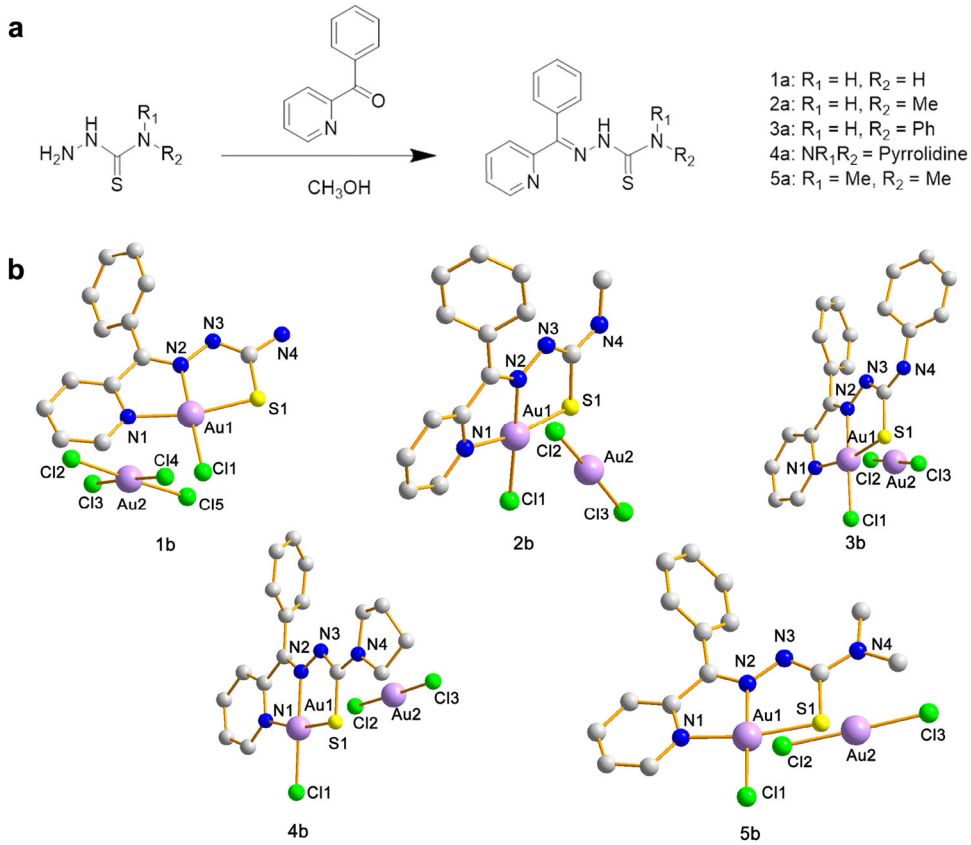

Fig. 1 Structures of 2-benzoylpyridine thiosemicarbazone compounds (1a–5a) and corresponding Au(III) complexes (1b–5b)

Table 1 IC_{50} (μM) values of 2-benzoylpyridine thiosemicarbazone compounds (1a–5a) and corresponding Au(III) complexes (1b–5b)

Complex	T98G	143B	A375	SK-OV-3	HK-2
1a	> 50	> 50	> 50	> 50	> 50
2a	> 50	46.32 ± 3.78	> 50	> 50	> 50
3a	40.26 ± 4.01	37.23 ± 3.52	> 50	35.78 ± 1.22	> 50
4a	30.65 ± 3.45	32.55 ± 3.01	> 50	30.43 ± 1.22	> 50
5a	28.66 ± 2.32	21.68 ± 1.98	39.23 ± 2.09	20.55 ± 1.05	> 50
1b	19.46 ± 1.96	23.01 ± 1.22	21.07 ± 1.87	17.43 ± 1.02	> 50
2b	12.36 ± 1.12	12.25 ± 1.01	12.28 ± 1.75	11.30 ± 0.78	42.55 ± 2.78
3b	9.02 ± 1.09	7.65 ± 0.92	10.23 ± 0.99	8.75 ± 0.54	30.24 ± 1.99
4b	3.24 ± 0.79	3.55 ± 0.46	4.05 ± 0.89	2.89 ± 0.99	16.55 ± 1.42
5b	1.94 ± 0.45	1.75 ± 0.34	1.88 ± 0.75	1.05 ± 0.68	12.44 ± 1.21
$Na[AuCl_4]\cdot 2H_2O$	> 50	> 50	> 50	> 50	> 50

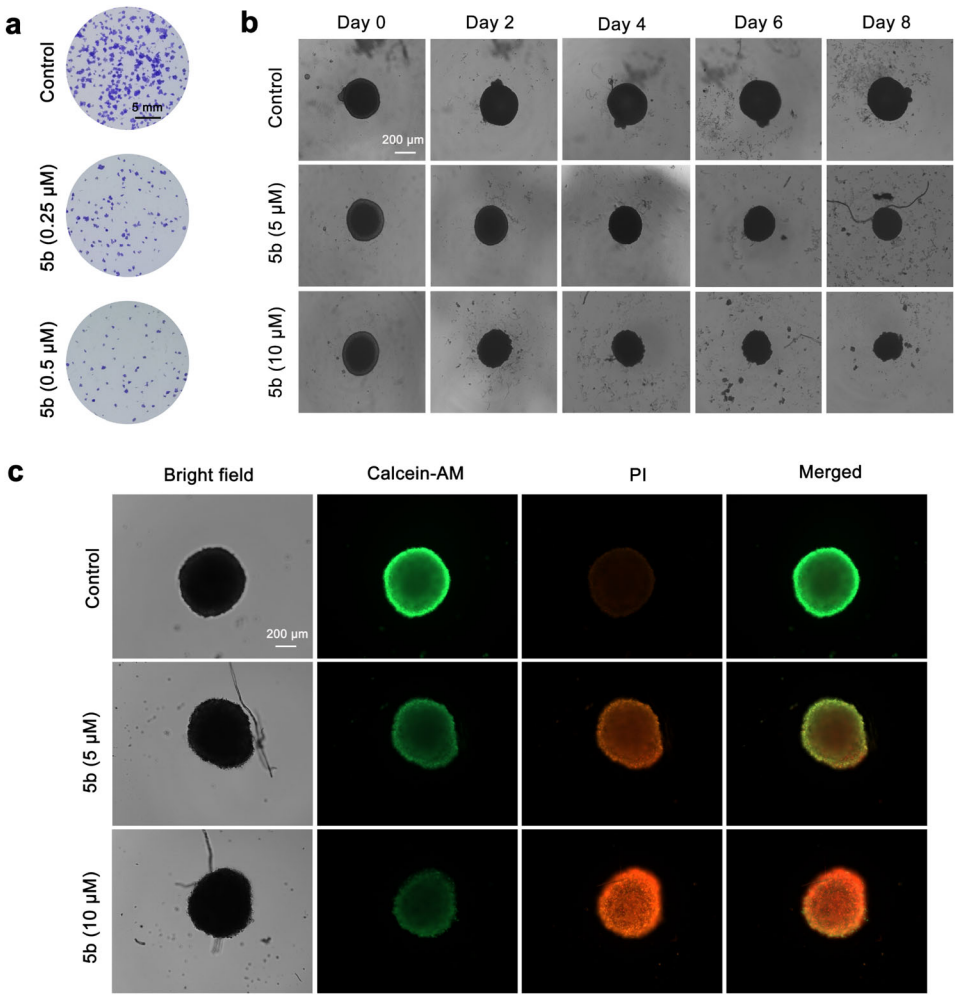

Fig. 2 In vitro antiproliferative activity of 5b: **a** colony formation of SK-OV-3 cells treated with 5b; **b** inhibitory effect of 5b on SK-OV-3 MCSs over 8 days; **c** Calcein-AM and PI dual staining of 5b-treated SK-OV-3 MCSs

surface of the tumor spheres were apoptotic. Then they gradually fell off, indicating that 5b had excellent anti-cancer activity.

To further determine the viability of MCSs, a calcein-AM and propidium iodide (PI) dual staining assay was carried out. Obviously, almost all cells in the control group were alive, as demonstrated by the green fluorescence of calcein-AM. In contrast, treatment with 5b induced massive cell death in the MCSs, as demonstrated by the red fluorescence of PI staining (Fig. 2c).

3.4 In vitro anti-metastatic activity of 5b

To explore the effects of 5b on tumor metastasis in vitro, we performed scratch wound healing and Transwell assays to simulate the process of cell migration and repair ability on SK-OV-3 cells. Figure 3a shows that cells in the control group migrate rapidly by time interval owing to the metastatic property. In contrast, the cells treated with 5b (1 and 2 μM) did not migrate toward the wounded side at such a swift rate and remained unchanged in the cells. Metastasis-associated colon cancer1 (MACC1) is a gene related to tumor invasion and metastasis. The downregulation of MACC1 expression level further indicated that 5b inhibited the cell metastasis (Fig. 3b, c). In addition, the Transwell assay was used to evaluate the chemotaxis ability of SK-OV-3 cells with three-dimensional migration (Fig. 3d). Upon the treatment of 5b, the invasion of the SK-OV-3 cells was significantly inhibited. Altogether, 5b could inhibit the invasion and migration ability of SK-OV-3 cells.

3.5 In vivo anti-tumor behavior of 5b.

3.4.1 In vivo biosafety of 5b

Concerns about biosafety always accompany metal-based drug therapy. To evaluate the biosafety of 5b in vivo, blood samples from mice were collected to detect the level of serum BUN/CRE (renal function) and serum ALT/AST (liver function) after intravenous (*i.v.*) injection with 5b at a dose of 2 or 4 μmol·kg^{-1}. The above parameters in the blood samples showed no obvious differences between the NaCl and 5b treatment groups (Table S3), indicating that 5b had no significant nephrotoxicity and liver toxicity.

3.4.2 In vivo therapeutic efficacy of 5b

In vivo therapeutic efficacy of 5b was evaluated by establishing SK-OV-3 tumor xenograft models. In the SK-OV-3 tumor model, the mice were treated via *i.v.* injection every 2 days with 5b at a dose of 2 or 4 μmol·kg^{-1} once the tumor reached a volume of 80 mm^3. At the end of treatment, the mice were euthanized, and tumor weight was

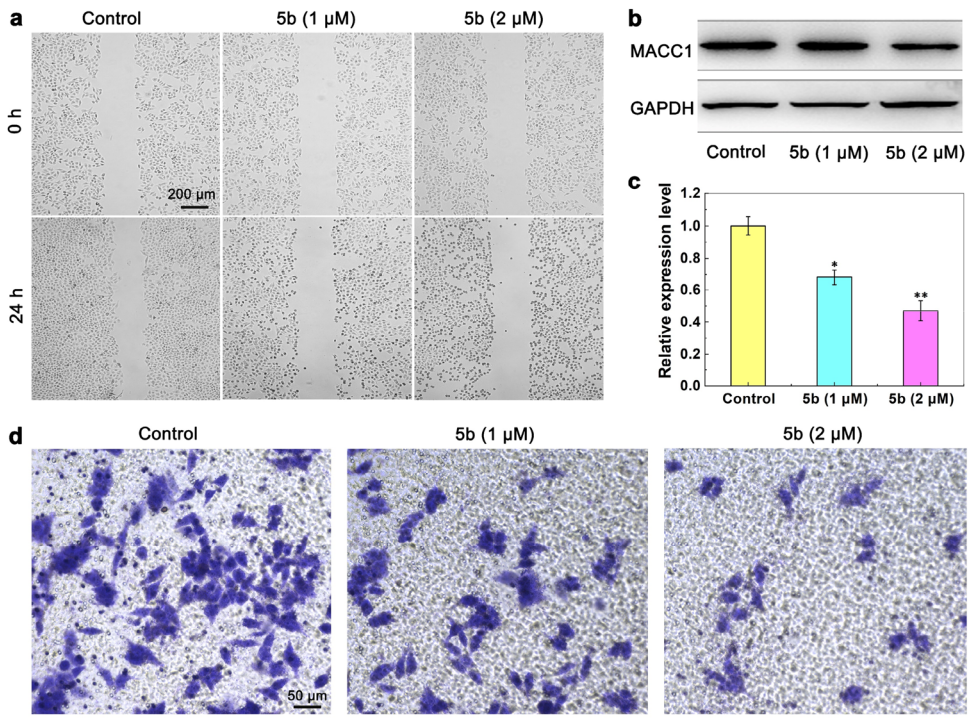

Fig. 3 Anti-metastatic function of complex 5b in vitro: **a** scratch wound healing of SK-OV-3 cells after treatment with 5b; **b**, **c** protein levels of MACC1 after treatment with 5b; **d** invasion of SK-OV-3 cells after different treatments as determined by Transwell assay (*$p < 0.05$)

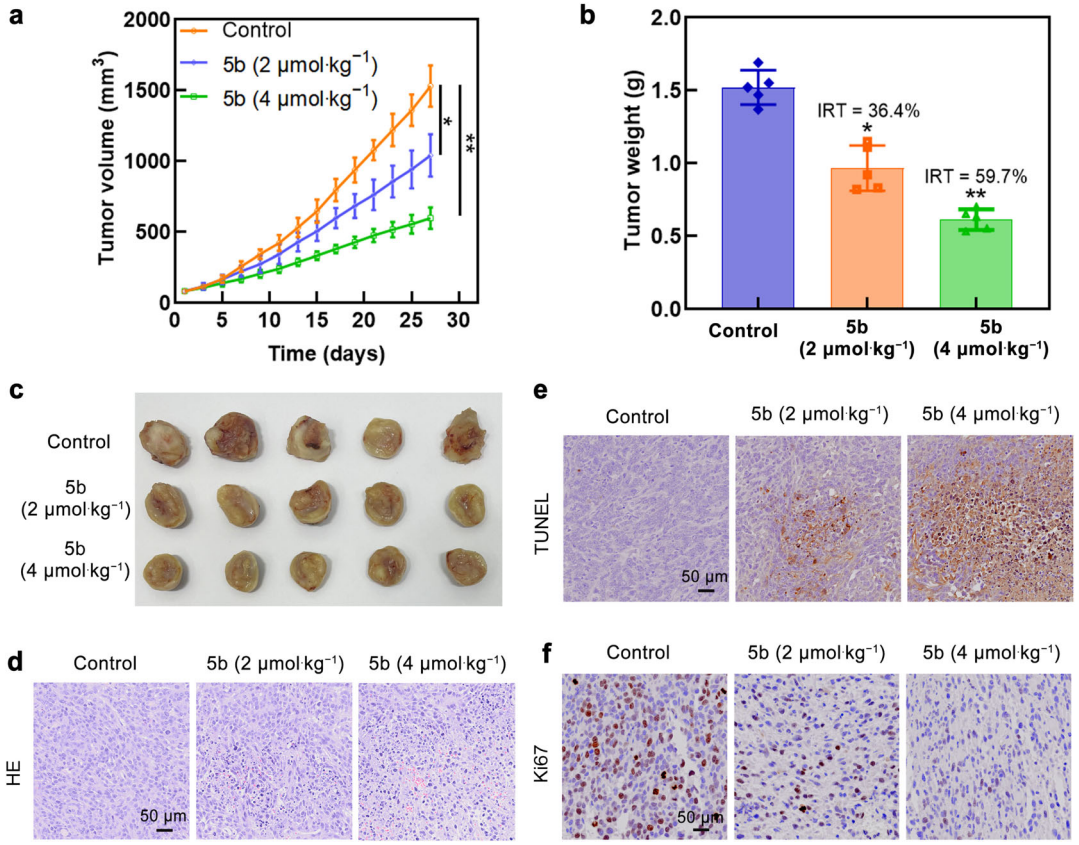

Fig. 4 Anti-tumor function of 5b in vivo: **a** tumor volumes, **b** tumor weights and **c** representative tumor tissue of mice treated with NaCl, 5b (2 μmol·kg^{-1}) and 5b (4 μmol·kg^{-1}); **d** HE staining; **e** TUNEL staining; **f** Ki67 staining in NaCl and 5b treatment groups (*$p < 0.05$, **$p < 0.01$)

measured. As displayed in Fig. 4a-c, complex 5b showed remarkable therapeutic efficacy in vivo, and the inhibition rate of tumor growth (IRT) was 59.7% at a dose of 4 μmol·kg^{-1}.

In addition, H&E staining of the tumor tissues showed that more necrosis regions were observed after treatment with 5b, indicating that 5b could effectively cause tumor cell death in vivo (Fig. 4d). Further studies were conducted via TUNEL. Treatment with 5b considerably increased the percentage of apoptotic or necrotic tumor cells compared with the control group (Fig. 4e). Furthermore, Ki67 immunostaining demonstrated that 5b could remarkably decrease tumor cell proliferation (Fig. 4f).

3.4.3 Side effects of 5b in vivo

For an in vivo evaluation of the side effects of complex 5b, the body weight of the mice was measured during treatment. As presented in Fig. 5a, there was no significant difference between the control and 5b groups. In addition, weighting and H&E staining were performed on the major organs of the mice at the end of treatment. Figure 5b, c shows that the major organ weights of those treated with 5b were similar to those of the control group. Moreover, H&E staining did not show apparent pathological lesions, indicating that the intratumoral administration of 5b was biocompatible.

3.5 Anti-metastatic behavior of 5b in vivo

Cell migration plays an essential role in embryogenesis, wound healing and the development of the immune response. However, it also leads to cancer cell invasion and metastasis [22]. To evaluate the effect of 5b on tumor metastasis in vivo, living SK-OV-3 cells were *i.v.* injected into mice to establish a model of lung metastasis. The lungs of the mice were harvested at the end of treatment and photographed after Bouin's staining, and the tumor metastatic nodules of each group of lungs were counted. The mice treated with 5b displayed fewer metastatic lesions in the whole lung, while numerous metastatic foci were observed in the control group (Fig. 6a). H&E staining further demonstrated that the numbers and sizes of dark dyed nodules with clear edges in the 5b group obviously decreased compared to those in the control group (Fig. 6b, c). Furthermore, after treatment with 5b, the weight of the lungs

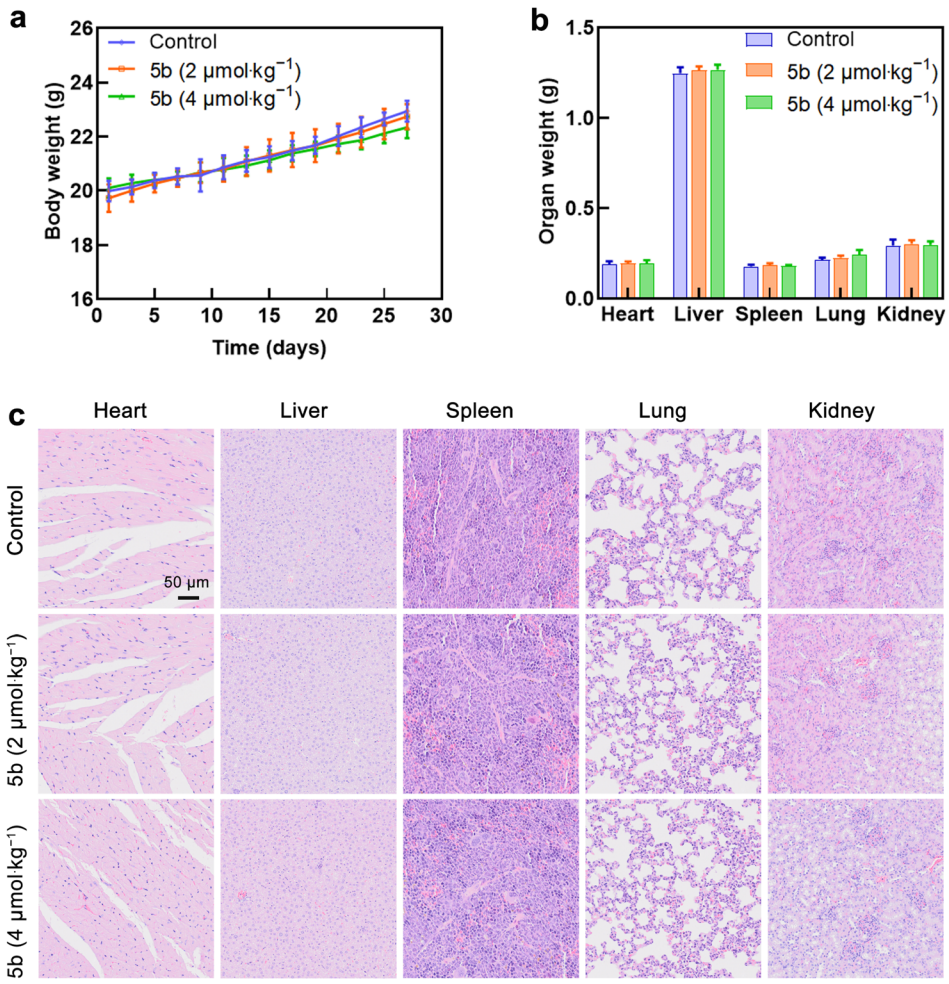

Fig. 5 Side effects of 5b in vivo: a body weight differences after treatment with NaCl, 5b (2 μmol·kg^{-1}) and 5b (4 μmol·kg^{-1}); **b** major organ weights of mice after treatment; **c** H&E staining of major organs of mice after treatment

decreased (Fig. 6d). These results indicated that 5b could effectively inhibit tumor metastasis in vivo.

3.6 Anticancer mechanism of 5b

3.6.1 Releasing ICD-associated DAMPs and activating immune response

Accumulating evidence indicates that many conventional chemotherapeutic drugs not only kill cancer cells directly based on their cytotoxicity but also achieve it by activating the tumor's immune system [23, 24]. To confirm whether 5b could activate the antitumor immune response induced by ICD, the release or exposure of ICD-associated DAMPs were detected. Upon treatment with 5b, the exposure of CRT on the cell membrane of SK-OV-3 cells was demonstrated by green immunofluorescence on the cell surface, while confocal laser scanning microscopy (CLSM) analysis of the control group revealed no surface expression of CRT (Fig. 7a). In addition, from the results of immunofluorescence staining results determined by CLSM, HMGB1 migrated from the nucleus to the cytoplasm or extracellular environment following 5b treatment in SK-OV-3 cancer cells (Fig. 7b). In line with this, the secretion of ATP in the supernatant significantly increased after treatment with 5b, as determined by a bioluminescence detection kit (Fig. 7c).

Subsequently, to investigate 5b-induced DAMPs release in vivo, mice bearing SK-OV-3 tumors received an *i.v.* injection of 5b. As shown in Fig. 7d, increased CRT exposure and HMGB1 release were visualized after treatment with 5b, as determined by immunofluorescence staining of the tumor tissue. Altogether, these results indicated that 5b could induce a strong release of ICD-associated DAMPs in vitro and in vivo, including cell surface exposure of CRT, migration of HMGB1 to the

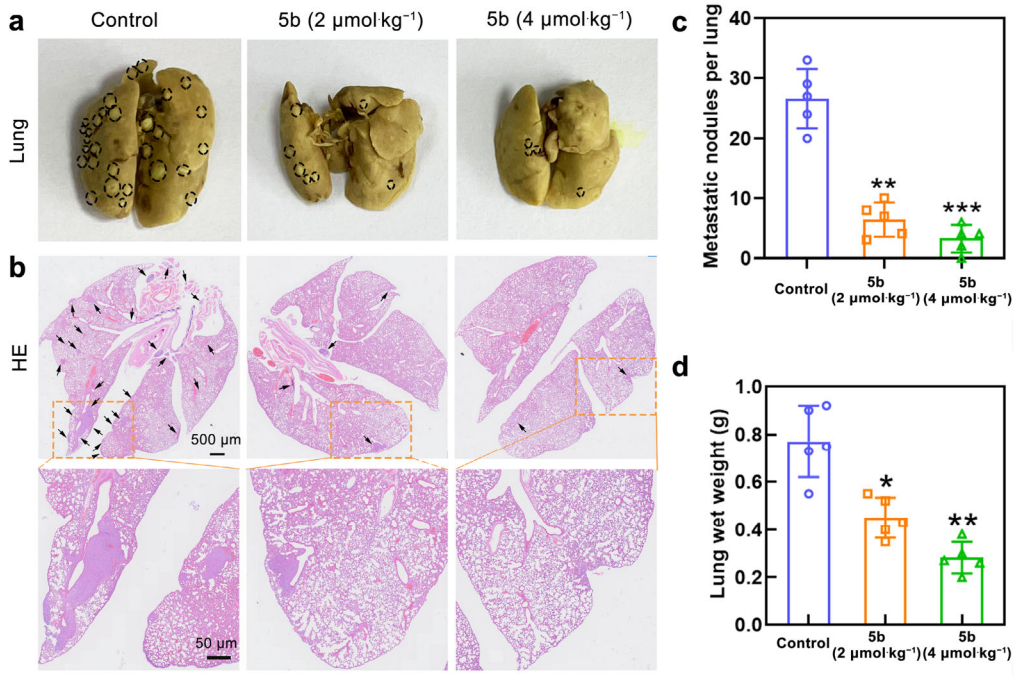

Fig. 6 Anti-metastatic function of complex 5b in vivo: **a** tumor metastatic nodules on lungs; **b** H&E staining of lungs of mice (black circles and arrows denote metastatic nodules); **c** number of metastatic nodules in each lung; **d** lung wet weights of mice after treatment (*$p < 0.05$, **$p < 0.01$, ***$p < 0.001$)

extracellular environment, and the secretion of large amounts of ATP.

ICD can stimulate the maturation of DCs, which can present the tumor-related antigens to T cells and then activate immune responses [25]. To verify whether the release of ICD-associated DAMPs could stimulate the maturation of DCs, we performed immunofluorescence staining to examine the expression of costimulatory molecule CD86 (a marker of DC maturation) in the tumor tissue after 5b treatment. Elevated expression of CD86 on the cell surface in a dose-dependent manner was observed in the tumor tissue (Fig. 7e).

Subsequently, immunofluorescence staining was performed to verify whether the matured DCs could activate the immune response by activating T lymphocytes. The results showed increased tumor-infiltrating $CD8^+$ T cells and decreased tumor-infiltrating regulatory T cells ($Fox-p3^+$) in the tumor tissue of the mice after injection with 5b (Fig. 7f). Collectively, 5b treatment could stimulate the maturation of DCs and activate the immune response.

3.6.2 *Inducing ERS and generating ROS*

Growing evidence indicates that the ability to cause ERS and ROS is closely related to the capacity to induce ICD by chemotherapeutic drugs [16]. We thus investigated whether 5b could induce ERS in SK-OV-3 cells. Phosphorylated eukaryotic initiation factor 2α (phospho-eIF2α), a hallmark of the stress response induced by ERS, significantly increased after 5b treatment, as determined by western blotting (Fig. 8a, b). Correspondingly, the activation of phosphorylated RNA-dependent protein kinase-like endoplasmic reticulum kinase (PERK) and overexpression of C/EBP homologous protein (CHOP) demonstrated that 5b could result in ERS and induce ER-related cell apoptosis.

In addition, glucose-regulated protein-78 (GRP78), an unfolded protein response indicator, serves as a gatekeeper for the ERS activation [26]. To further verify the existence of ERS, the immunofluorescence staining of GRP78 on SK-OV-3 cells after treatment was carried out. Based on the results illustrated in Fig. 8c, few fluorescence signals were observed in the control group, while bright fluorescence was exhibited in the 5b treatment group, indicating that 5b induced ERS. Transmission electron microscopy (TEM) was then used to intuitively investigate the morphological changes of the ER in SK-OV-3 cells after 5b treatment. As shown in Fig. 8d, untreated SK-OV-3 cells (control) showed the familiar appearance of the smooth ER (orange arrow). In contrast, the ER in SK-OV-3 cells treated with 5b became swollen (orange arrow), suggesting

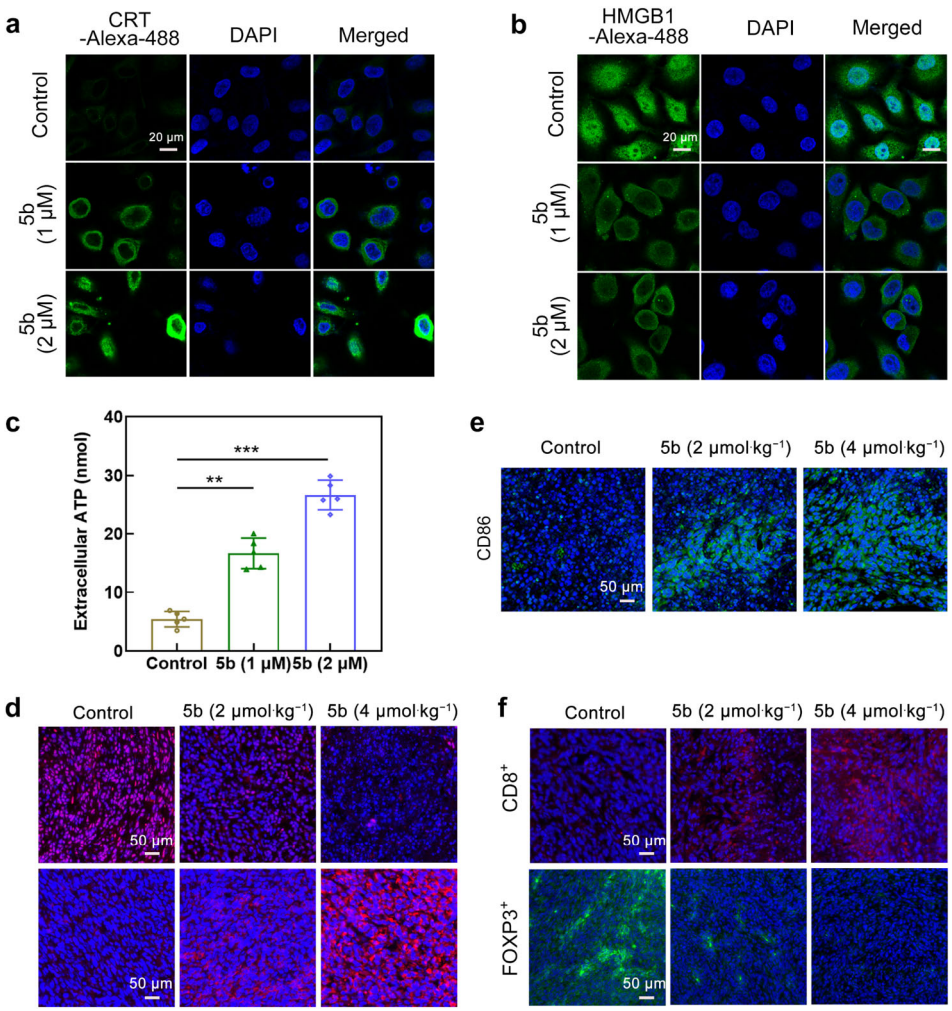

Fig. 7 Treatment with 5b released ICD-associated DAMPs and activated immune response: **a** exposure of CRT and **b** release of HMGB1 analyzed by immunofluorescence in SK-OV-3 cells after 5b treatment; **c** extracellular ATP levels of SK-OV-3 cells after 5b treatment; **d** exposure of CRT (up) and release of HMGB1 (down) analyzed by immunofluorescence in tumor tissues after 5b treatment; immunofluorescence analysis of expression of **e** CD86 and **f** $CD8^+$ and $FOXP3^+$ in tumor tissues after 5b treatment (**$p < 0.01$, ***$p < 0.001$)

misfolded protein accumulation in the ER. The results above suggested that 5b might have an anticancer mechanism involving ERS.

Subsequently, to verify whether the ERS response was mediated by ROS, we used DCFH-DA and ER-Tracker Red as ROS and ER indicators, respectively. It was shown that there was co-localization between the ER and ROS after 5b treatment at a concentration of 1 μM. ROS became diffuse with increasing concentration of 5b, the ER suffered severe deformation, and the co-localization of ROS with ER gradually decreased, which might have been caused by the increase in ER membrane permeability (Fig. 8e). Furthermore, severe ERS is highly associated with the disturbance of Ca^{2+} homeostasis in the ER [27]. The data in Fig. 8f confirmed that compared with the control group, the cells treated with 5b showed more green fluorescence labeling by the Ca^{2+} indicator Fluo-4 AM, indicating the imbalance of the Ca^{2+} concentration in the SK-OV-3 cells.

3.6.3 *Inducing mitochondrial dysfunction and promoting mitophagy*

The ERS response is highly associated with oxidative stress [28]. The release of Ca^{2+} from the ER caused by severe ERS is absorbed by mitochondria, which stimulates the generation of excessive ROS in mitochondria, thereby inducing mitochondrial dysfunction. A loss of mitochondrial membrane potential ($\Delta\Psi_m$) was observed via flow cytometry (Fig. S2) and CLSM (Fig. 9a), indicating that 5b

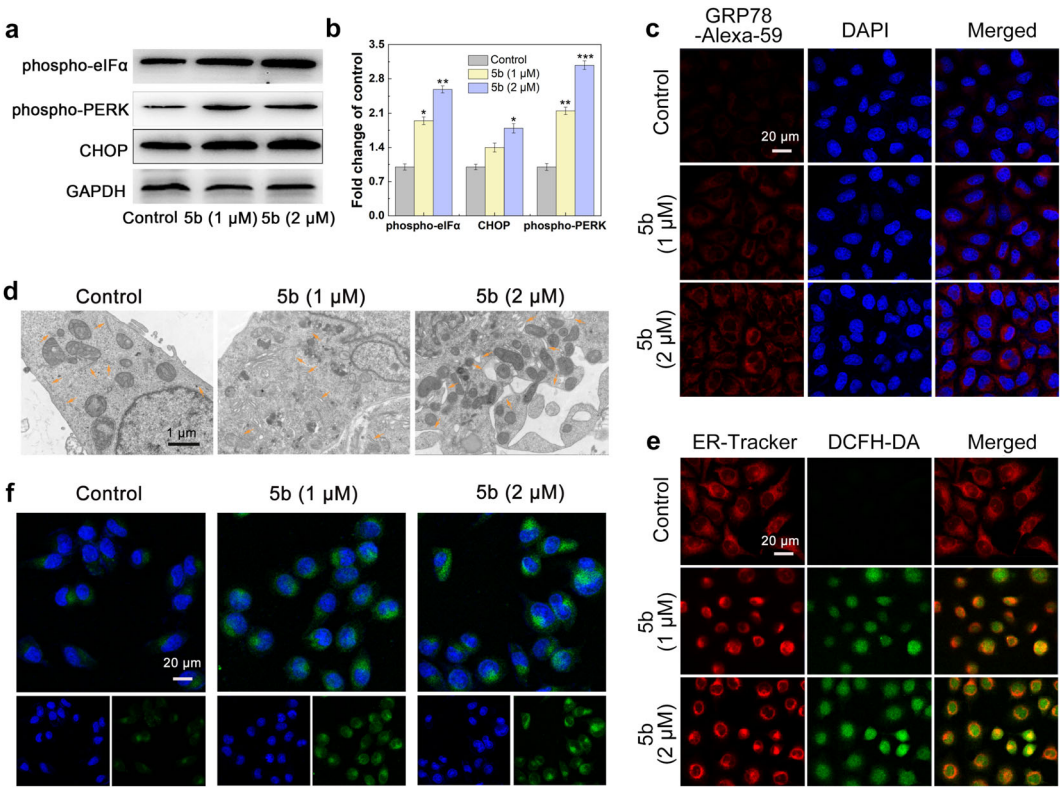

Fig. 8 ERS induced by 5b treatment: **a**, **b** protein levels of phospho-eIF2α, phosphor-PERK and CHOP after 5b treatment for 48 h; **c** immunofluorescence analysis of GRP78 after 5b treatment; **d** typical TEM images of endoplasmic reticulum morphology of SK-OV-3 cells treated with 5b; **e** ROS analyzed by DCF-DA and ER analyzed by ER-Tracker Red by binding to Sulfonylurea receptor in ER; **f** release of Ca^{2+} analyzed by Fluo 4-AM after 5b treatment (*$p < 0.05$, **$p < 0.01$, ***$p < 0.001$)

induced an increase in mitochondrial outer membrane permeability (MOMP), which could damage the mitochondria permanently, release cytochrome c into the cytosol, and eventually lead to apoptosis.

Excessive damage to the mitochondria often triggers mitophagy to maintain extrinsic homeostasis in cells and increase the secretion of ATP [29]. To examine whether autophagosomes engulfed the dysfunctional mitochondria in 5b-treated SK-OV-3 cells, we analyzed the co-localization of autophagosomes instructed by light chain 3 (LC3) and the mitochondria. It was shown that the colocalization of the mitochondria and autophagosomes increased, as evidenced by the merged fluorescence signaling of LC3 (green) and Mito-Tracker (red) (Fig. 9b), indicating that 5b could promote mitophagy. Further evidence of autophagy is shown in Fig. 9c, d, as determined by western blotting showing the up-regulation of Beclin 1 and downregulation of p62 dose-dependently after 5b treatment. Altogether, 5b induced severe mitochondrial damage and promoted mitophagy in the SK-OV-3 cells.

Furthermore, the annexin-V/propodeum iodide double staining assay showed that after 5b treatment, the percentage of apoptotic cells increased to 37.09% (1 μM of 5b) and 45.05% (2 μM of 5b) (Fig. 9e). The expression level of apoptosis-related proteins, as determined by western blotting, showed that 5b elevated the cytochrome c, Bax, Bad, P53 and Apaf-1 levels, but decreased the anti-apoptosis protein expressions (Bcl-2 and Bcl-xl) (Fig. S3), indicating that 5b treatment eventually induced cell apoptosis.

4 Discussion

Cisplatin is well-known as a first-line chemotherapeutic agent for treating of various cancers, which can promote the generation of ROS, and then induce ERS and nucleus-dependent apoptosis [30]. However, unlike other chemotherapeutic agents such as oxaliplatin and anthracyclines that can induce ICD through ERS, *cisplatin*-induced death is typically immunologically silent [31]. Therefore, it is one of the most effective strategies for overcoming the shortcomings of *cisplatin* with the design of a metal complex based on novel mechanisms to reverse immune tolerance. Herein, we proposed to design an Au(III) thiosemicarbazone complex to kill cancer cells via chemotherapy and immunotherapy. Indeed, our results

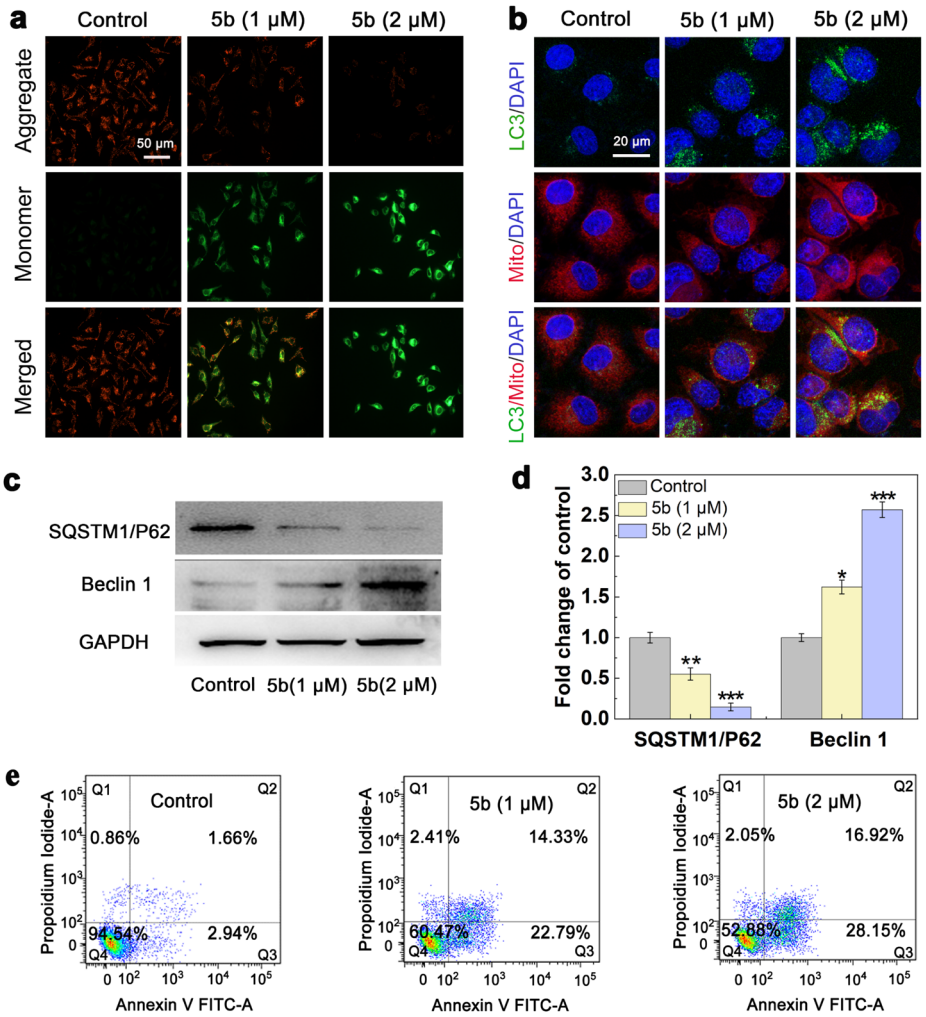

Fig. 9 5b induced mitochondrial dysfunction and promoted mitophagy: **a** loss of MMP in SK-OV-3 cells after 5b treatment; **b** SK-OV-3 cells treated with 5b stained with Mito Tracker (Red) and immunofluorescence stained with LC3 (green); **c**, **d** protein levels of SQSTM1/P62 and Beclin1 after 5b treatment for 48 h; **e** apoptosis of SK-OV-3 cells after 5b treatment (*$p < 0.05$, **$p < 0.01$, ***$p < 0.001$)

provided solid evidence to support our hypothesis that 5b released ICD-associated DAMPs, including cell surface exposure of CRT, migration of HMGB1 to the extracellular environment and the secretion of large amounts of ATP, stimulated DC maturation and then activated the immune response (Fig. 7). Interestingly, we also revealed the mechanisms by which 5b induces ICD. The results showed that 5b induced strong ERS and released Ca^{2+} from the ER, which caused the loss of $\Delta\Psi_m$ and stimulated the generation of excessive ROS in the mitochondria. A combination of massive Ca^{2+}, loss of $\Delta\Psi_m$ and excessive ROS indicated that 5b initiated MOMP, which can permanently damage the mitochondria and induce strong ERS (Figs. 8, 9) [32]. Eventually, this triggered the massive release of ICD-associated DAMPs and the activation of the immune response toward ovarian cancer. Obviously, 5b is worthwhile to develop as a promising next-generation lead metal agent because it kills ovarian cancer cells by inducing ERS and mitochondrial dysfunction-driven ICD (Fig. 10).

The antitumor activity of 5b was evaluated by establishing SK-OV-3 tumor xenograft models. The results showed that 5b considerably inhibited tumor growth because its IRT was 59.7%. Notably, no apparent side effects were observed during the treatment. Furthermore, fewer metastatic nodules in the 5b groups were observed compared to the control group, indicating that 5b could effectively inhibit metastasis. Thus, 5b not only exhibited excellent inhibition of tumor growth with fewer side effects in ovarian cancer, but also effectively inhibited metastasis.

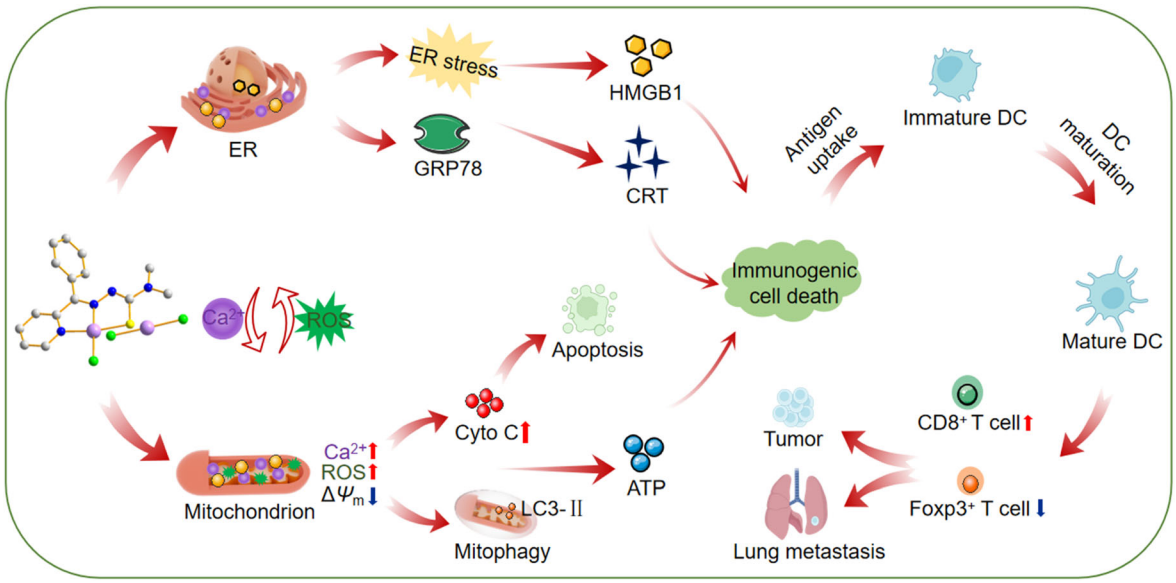

Fig. 10 Anticancer mechanisms of 5b inhibition tumor growth and metastasis via integration of chemotherapy with immunotherapy

5 Conclusion

To effectively inhibit tumor growth and metastasis for cancer treatment, a novel Au(III) 2-benzoylpyridine thiosemicarbazone complex (5b) was designed and synthesized. 5b not only induced ERS and ROS generation, but also caused severe mitochondrial damage, followed by the release of ICD-related DAMPs and the activation of the immune response. Meanwhile, 5b effectively inhibited tumor metastasis in vitro and in vivo. Obviously, our studies provides a potential new immunotherapy for ovarian cancer with the development of the Au(III) thiosemicarbazone complex, which acts as an ICD inducer.

Acknowledgements This work was financially supported by the Natural Science Foundation of Guangxi (No. 2022GXNSFGA035003) and the National Natural Science Foundation of China (No. 22077021).

Declarations

Conflict of interests The authors declare that they have no conflict of interest.

References

[1] Mullard A. Addressing cancer's grand challenges. Nat Rev Drug Discov. 2020;19(12):825. https://doi.org/10.1038/d41573-020-00202-0.

[2] Ghosh S. Cisplatin: the first metal based anticancer drug. Bioorg Chem. 2019;88:102925. https://doi.org/10.1016/j.bioorg.2019.102925.

[3] Xiong J, Wu M, Chen J, Liu Y, Chen Y, Fan G, Liu Y, Cheng J, Wang Z, Wang S, Liu Y, Zhang W. Cancer-erythrocyte hybrid membrane-camouflaged magnetic nanoparticles with enhanced photothermal-immunotherapy for ovarian cancer. ACS Nano. 2021;15(12):19756. https://doi.org/10.1021/acsnano.1c07180.

[4] Alzeibak R, Mishchenko TA, Shilyagina NY, Balalaeval IV, Vedunova MV. Krysko DV targeting immunogenic cancer cell death by photodynamic therapy: past, present and future. J Immunother Cancer. 2021;9(1):e001926. https://doi.org/10.1136/jitc-2020-001926.

[5] Li Z, Lai X, Fu S, Ren L, Cai H, Zhang H, Gu Z, Ma X, Luo K. Immunogenic cell death activates the tumor immune microenvironment to boost the immunotherapy efficiency. Adv Sci (Weinh). 2022;9(22):e2201734. https://doi.org/10.1002/advs.202201734.

[6] Tang R, Xu J, Zhang B, Liu J, Liang C, Hua J, Meng Q, Yu X, Shi S. Ferroptosis, necroptosis, and pyroptosis in anticancer immunity. J Hematol Oncol. 2020;13(1):110. https://doi.org/10.1186/s13045-020-00946-7.

[7] Wang Q, Ju X, Wang J, Fan Y, Ren M, Zhang H. Immunogenic cell death in anticancer chemotherapy and its impact on clinical studies. Cancer Lett. 2018;438:17. https://doi.org/10.1016/j.canlet.2018.08.028.

[8] Sen S, Won M, Levine MS, Noh Y, Sedgwick AC, Kim JS, Sessler JL, Arambula JF. Metal-based anticancer agents as immunogenic cell death inducers: the past, present, and future. Chem Soc Rev. 2022;51(4):1212. https://doi.org/10.1039/d1cs00417d.

[9] Li F, Wen Z, Wu C, Yang Z, Wang Z, Diao W, Chen D, Xu Z, Lu Y, Liu W. Simultaneous activation of immunogenic cell death and cGAS-STING pathway by liver- and mitochondria-targeted Gold(I) complexes for chemoimmunotherapy of hepatocellular carcinoma. J Med Chem. 2024;67(3):1982. https://doi.org/10.1021/acs.jmedchem.3c01785.

[10] Yang Z, Bian M, Lv L, Chang X, Wen Z, Li F, Lu Y, Liu W. Tumor-targeting NHC–Au(I) complex induces immunogenic cell death in hepatocellular carcinoma. J Med Chem. 2023;66(6):3934. https://doi.org/10.1021/acs.jmedchem.2c01798.

[11] Sen S, Hufnagel S, Maier EY, Aguilar I, Selvakumar J, DeVore JE, Lynch VM, Arumugam K, Cui Z, Sessler JL, Arambula JF Rationally designed redox-active Au(I) N-Heterocyclic carbene: an immunogenic cell death inducer. J. Am. Chem. Soc. 2020;142(49):20536. https://doi.org/10.1021/jacs.0c09753

[12] Xiong X, Wang Y, Zou T. Towards understanding the molecular mechanisms of immunogenic cell death. ChemBioChem. 2022; 24(6):e202200621. https://doi.org/10.1002/cbic.202200621.
[13] Xiong X, Huang K-B, Wang Y, Cao B, Luo Y, Chen H, Yang Y, Long Y, Liu M, Chan ASC, Liang H, Zou T. Target profiling of an iridium(III)-based immunogenic cell death inducer unveils the engagement of unfolded protein response regulator BiP. J Am Chem Soc. 2022;144(23):10407. https://doi.org/10.1021/jacs.2c02435.
[14] Kaur P, Johnson A, Northcote-Smith J, Lu C, Suntharalingam K. Immunogenic cell death of breast cancer stem cells induced by an endoplasmic reticulum-targeting copper(II) complex. ChemBioChem. 2020;21(24):3618. https://doi.org/10.1002/cbic.202000553.
[15] Ma H, Lu Y, Huang Z, Long S, Cao J, Zhang Z, Zhou X, Shi C, Sun W, Du J, Fan J, Peng X. ER-targeting cyanine dye as an NIR photoinducer to efficiently trigger photoimmunogenic cancer cell death. J Am Chem Soc. 2022;144(8):3477. https://doi.org/10.1021/jacs.1c11886.
[16] Wang L, Guan R, Xie L, Liao X, Xiong K, Rees TW, Chen YJiL, Chao H. An ER-targeting iridium(III) complex that induces immunogenic cell death in non-small-cell lung cancer. Angew Chem IntEd Engl 2021;60(9):4657 https://doi.org/10.1002/anie.202013987.
[17] Zhang Z, Zhang J, Yang TLiS, Xu G Liang H Yang F. Developing an anticancer platinum (II) compound based on the uniqueness of human serum albumin. J Med Chem 2023;66(8): 5669 https://doi.org/10.1021/acs.jmedchem.3c00001
[18] Man X, Yang T, Li W, Li S, Xu G, Zhang Z, Liang H, Yang F. Developing a Gadolinium(III) compound based on apoferritin for targeted magnetic resonance imaging and dual-modal therapy of cancer. J Med Chem. 2023;66(11):7268. https://doi.org/10.1021/acs.jmedchem.2c01904.
[19] Li W, Li S, Zhang Z, Xu G, Man X, Yang F, Liang H. Developing a multitargeted anticancer palladium(II) agent based on the His-242 residue in the IIA subdomain of human serum albumin. J Med Chem. 2023;66(13):8564. https://doi.org/10.1021/acs.jmedchem.3c00248.
[20] Matesanz AI, Herrero JM, Quiroga AG. Chemical biological evaluation of thiosemicarbazone-bearing heterocyclic metal complexes. Curr Top Med Chem. 2021;21(1):59. https://doi.org/10.2174/1568026620666201022144004.
[21] Li W, Li S, Xu G, Man X, Yang T, Zhang Z, Liang H, Yang F. Developing a ruthenium(III)complex to trigger gasdermin E--mediated pyroptosis and an immune response based on decitabine and liposomes: targeting inhibition of gastric tumor growth and metastasis. J Med Chem. 2023;66(18):13072. https://doi.org/10.1021/acs.jmedchem.3c01110.
[22] Friedl P, Alexander S. Cancer invasion and the microenvironment: plasticity and reciprocity. Cell. 2011;147(5):992. https://doi.org/10.1016/j.cell.2011.11.016.
[23] Bian M, Fan R, Yang Z, Chen Y, Xu Z, Lu Y, Liu W. Pt(II)-NHC complex induces ROS-ERS-related DAMP balance to harness immunogenic cell death in hepatocellular carcinoma. J Med Chem. 2022;65(3):1848. https://doi.org/10.1021/acs.jmedchem.1c01248.
[24] Englinger B, Pirker C, Heffeter P, Terenzi A, Kowol CR, Keppler BK, Berger W. Metal drugs and the anticancer immune response. Chem Rev. 2019;119(2):1519. https://doi.org/10.1021/acs.chemrev.8b00396.
[25] Krysko DV, Garg AD, Kaczmarek A, Krysko O, Agostinis P, Vandenabeele P. Immunogenic cell death and DAMPs in cancer therapy. Nat Rev Cancer. 2012;12(12):860. https://doi.org/10.1038/nrc3380.
[26] Samanta S, Yang S, Debnath B, Xue D, Kuang Y, Ramkumar K, Lee AS, Ljungman M, Neamati N. The hydroxyquinoline analogue YUM70 inhibits GRP78 to induce ER stress-mediated apoptosis in pancreatic cancer. Cancer Res. 2021;81(7):1883. https://doi.org/10.1158/0008-5472.CAN-20-1540.
[27] Park SW, Zhou Y, Lee J, Lee J, Ozcan U. Sarco(endo)plasmic reticulum Ca^{2+}-ATPase 2b is a major regulator of endoplasmic reticulum stress and glucose homeostasis in obesity. Proc Natl Acad Sci U S A. 2010;107(45):19320. https://doi.org/10.1073/pnas.1012044107.
[28] Lin Y, Jiang M, Chen W, Zhao T, Wei Y. Cancer and ER stress: Mutual crosstalk between autophagy, oxidative stress and inflammatory response. Biomed Pharmacother. 2019;118: 109249. https://doi.org/10.1016/j.biopha.2019.109249.
[29] Chipuk JE, Bouchier-Hayes L, Green DR. Mitochondrial outer membrane permeabilization during apoptosis: the innocent bystander scenario. Cell Death Differ. 2006;13(8):1396. https://doi.org/10.1038/sj.cdd.4401963.
[30] Romani AMP. Cisplatin in cancer treatment. Biochem. Pharmacology. 2022;206:115323. https://doi.org/10.1016/j.bcp.2022.115323.
[31] Ding F, Li F, Tang D, Wang B, Liu J, Mao X, Yin J, Xiao H, Wang J, Liu Z. Restoration of the immunogenicity of tumor cells for enhanced cancer therapy via nanoparticle-mediated copper chaperone inhibition. Angew Chem Int Ed Engl. 2022;61(31): e202203546. https://doi.org/10.1002/anie.202203546.
[32] Giampazolias E, Zunino B, Dhayade S, Bock F, Cloix C, Cao K, Roca A, Lopez J, Ichim G, Proïcs E, Rubio-Patiño C, Fort L, Yatim N, Woodham E, Orozco S, Taraborrelli L, Peltzer N, Lecis, Machesky L, Walczak H, Albert ML, Milling S, Oberst A, Ricci J-E, Ryan KM, Blyth K, Tait SWG. Mitochondrial permeabilization engages NF-κB-dependent anti-tumour activity under caspase deficiency. Nat Cell Bio 2017;19(9):1116 https://doi.org/10.1038/ncb3596

Springer Nature or its licensor (e.g. a society or other partner) holds exclusive rights to this article under a publishing agreement with the author(s) or other rightsholder(s); author self-archiving of the accepted manuscript version of this article is solely governed by the terms of such publishing agreement and applicable law.